COMPDYN 2015
5th ECCOMAS Thematic Conference on
Computational Methods in Structural Dynamics and Earthquake Engineering
M. Papadrakakis, V. Papadopoulos, V. Plevris (eds.)
Crete Island, Greece, 25–27 May 2015

SEISMIC VULNERABILITY IN CASE OF FIRE OF EXISTING R.C. FRAMED BUILDINGS: MODELLING AND NONLINEAR DYNAMIC ANALYSIS

Fabio Mazza[1] **and Antonio De Luca**[2]

[1]Dipartimento di Ingegneria Civile, Università della Calabria
Via P. Bucci, 87036 Rende (CS), Italy
fabio.mazza@unical.it

[2]Dipartimento di Ingegneria Civile, Università della Calabria
Via P. Bucci, 87036 Rende (CS), Italy
antonioodelucaa@alice.it

Keywords: R.C. Framed Structures, Fire Scenarios, Time-Temperature Curves, Thermal Mappings, Nonlinear Dynamic Analysis.

Abstract. *The seismic vulnerability of reinforced concrete (r.c.) framed buildings designed with inadequate seismic zone classifications and seismic code provisions is recognized to be a serious problem. Nevertheless, knowledge on the seismic response in the case of fire is lacking and an amplification of the structural damage is expected in the case of fire-exposed existing structures not designed to withstand fire. To evaluate the nonlinear seismic response following a fire, a numerical investigation is carried out with reference to a five-storey r.c. framed building, which, primarily designed according to the previous Italian seismic code (DM96) for a medium risk zone, needs to be considered as in a high-risk seismic zone provided by the current Italian seismic code (NTC08). More specifically, the nonlinear seismic response of the test structure in a no fire situation is compared with that in the event of fire, at 45 (i.e. R45) and 60 (i.e. R60) minutes of fire resistance, assuming damaged (i.e. DS) and repaired (i.e. RS) stiffness conditions. Five fire scenarios have been considered on the assumption that the fire compartment is confined to the area of the first level (i.e. F1), the first two (i.e. F1/2) and the upper (i.e. Fi, i=3-5) levels, with the parametric temperature-time fire curve evaluated in accordance with Eurocode 1. The nonlinear dynamic analysis is performed through a step-by-step procedure based on a two-parameter implicit integration scheme and an initial-stress-like iterative procedure. At each step of the analysis, plastic conditions are checked at the critical (end) sections of the girders and columns, where a thermal mapping with reduced mechanical properties is evaluated in line with the 500°C isotherm method proposed by Eurocode 2. Two sets of seven real motions, whose response spectra match on average NTC08 spectra for a subsoil class B, are considered with regard to high-risk seismic zone and two topographic classes.*

1 INTRODUCTION

Assessment of the seismic vulnerability of existing structures where fire safety is neglected represents a far-reaching problem especially in the case of reinforced concrete (r.c.) buildings designed for vertical loads only or with inadequate seismic zone classifications and code provisions. In the conventional aseismic design it is accepted that structures can withstand strong ground motions by mainly undergoing inelastic deformations. Consequently, fire can be a serious problem for a structure that has been partially damaged in a prior seismic event, because fire resistance will decrease [1]. More specifically, the fire response of r.c. frame members depends on the thermal (i.e. thermal conductivity, specific heat, thermal diffusivity and mass loss), mechanical (i.e. compressive and tensile strength, modulus of elasticity and stress-strain law) and deformation (i.e. thermal expansion and creep) properties of concrete and reinforcing steel bars, changing substantially with heating rate, strain rate and temperature gradient [2]. The combined effect of earthquake and fire has gained attention of recent studies into the nonlinear response of r.c. framed [3] and frame-wall [4] structures.

On the other hand, earthquakes following fires may find structures whose seismic resistance is considerably reduced. Numerical [5-7] and experimental [8, 9] studies have been carried out on the assessment of the residual seismic load capacity of r.c. structures, in terms of stiffness, strength and ductility after fire. In most cases of fire, structures experience degradation of material properties, due to high temperature, and damage to the structural members, from thermal expansion. In addition, fire induces spalling of concrete that can play a significant role in the seismic performance of r.c. frame members. However, despite the lack of knowledge on the seismic vulnerability of existing framed structures in the event of fire we can expect an amplification of the structural damage in the case of existing structures that have been exposed to fire.

In the present work, the nonlinear seismic response of r.c. framed structures in a no fire situation is compared with that in which fire has occurred, at 45 (i.e. R45) and 60 (i.e. R60) minutes of fire resistance, assuming both damaged (i.e. DS) and repaired (i.e. RS) stiffness conditions in the r.c. frame members. To this end, five-storey r.c. office buildings are designed in line with the previous Italian seismic code [10] for a medium risk zone. A numerical fire investigation is carried out considering a thermal-mechanical mapping analysis, with reduced mechanical properties evaluated in accordance with the 500°C isotherm method proposed by Eurocode 2 [11], followed by a sequentially uncoupled nonlinear dynamic analysis [12, 13]. In order to study the seismic response of the r.c. framed building damaged from fire, real ground motions corresponding to high-risk seismic intensity, provided by the current Italian seismic code [14], and different topographic conditions are considered. Five fire scenarios are hypothesized assuming the fire compartment confined to the area of the first level (i.e. F1), the first two (i.e. F1/2) and the upper (i.e. Fi, i=3-5) levels, with the parametric temperature-time fire curve evaluated in accordance with Eurocode 1 [15].

2 R.C. TEST STRUCTURE: DESIGN AND FIRE MODELLING

A typical five-storey office building with a r.c. framed structure, whose symmetric plan is shown in Figure 1a, is considered as test structure. Perimeter masonry infills, assumed as non-structural elements regularly distributed in elevation, are considered. For the sake of simplicity, the plane frames orientated along the horizontal ground motion direction (*Y*), perpendicular to the floor slab direction (*X*) shown in Figure 1a, are considered as a reference scheme. The dimensions of the cross sections assumed for the columns and the girders, equal at a given level and with a regular tapering in elevation, are reported in Figure 1b.

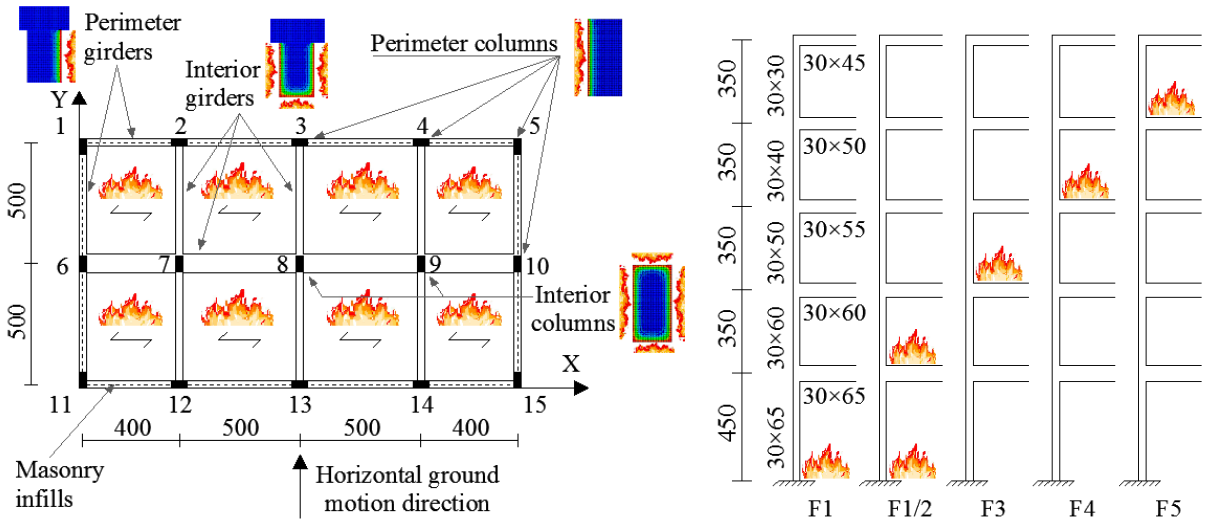

(a) Plan and fire compartment. (b) Elevation and fire scenarios.

Figure 1: R.c. test structure (dimensions in cm).

A simulated design of the test structure is carried out in line with the previous Italian seismic code (DM96, [10]), for a medium-risk seismic region (degree of seismicity S=9, which corresponds to a coefficient of seismic intensity C=0.07) and a typical subsoil class (subsoil parameter ε=1). The gravity loads are represented by a dead load of 4.48 kN/m^2 on the top floor and 5.18 kN/m^2 on the other floors, and a live load of 3.0 kN/m^2 on all the floors; infill walls, regularly distributed in elevation along the perimeter are considered, assuming an average weight of about 2.7 kN/m^2. A cylindrical compressive strength of 20 N/mm^2 for the concrete and a yield strength of 375 N/mm^2 for the steel are assumed for the r.c. frame members. The design complies with the ultimate limit states satisfying minimum conditions for the longitudinal bars of the girders and columns: at least two 12 mm bars are provided both at the top and bottom throughout the entire length of the frame members; for the girders, a tension reinforcement ratio not less than 0.37% (for the assumed yield strength) is provided and, at their end sections, a compression reinforcement not less than half of the tension reinforcement is placed; minimum steel geometric ratio is 1% for the symmetrically-reinforced section of each column. The dynamic properties of the six main vibration modes are reported in Table 1: i.e. vibration period (T_i); effective masses in the X ($m_{E,X}$) and Y ($m_{E,Y}$) directions, expressed as percentage of the total mass (m_{tot}).

Mode	T_i [s]	$m_{E,X}$ [%m_{tot}]	$m_{E,Y}$ [%m_{tot}]
1	0.808	81.6	0
2	0.749	0	80.4
3	0.326	13.0	0
4	0.302	0	13.5
5	0.195	3.4	0
6	0.183	0	3.8

Table 1: Dynamic properties of the test structure (m_{tot}= 9.35 kNs^2/cm).

Five fire scenarios have been reported in Figures 1a and 1b, assuming the fire compartment is confined to the area of the first level (i.e. F1), the first two (i.e. F1/2) and the upper (i.e. Fi, i=3-5) levels. It is worth noting that F1/2 fire scenario is obtained from F1 and F2, which occur simultaneously. The geometric properties of the fire compartment are reported in Table 2, for the first and the upper levels: i.e. L, D and H representing length, depth and height, respec-

tively; A_f, floor area; A_t, total area of enclosure (i.e. walls, ceiling and floor, including openings); A_v, total area of vertical openings; h_{eq}, weighted average height of windows. From these values it is possible to define an opening factor, representing the amount of ventilation:

$$O = A_v h_{eq}^{0.5} \Big/ A_t \tag{1}$$

Fire compartment	L [m]	D [m]	H [m]	A_f [m^2]	A_t [m^2]	A_v [m^2]	h_{eq} [m]	O [m$^{0.5}$]
First level	18	10	4.5	180	612	24	1.5	0.048
Upper levels	18	10	3.5	180	556	24	1.5	0.053

Table 2: Geometric properties of fire compartment.

Depending on combustible contents and relevant combustible parts of the building, the design value of the fire load density is defined as [15]:

$$q_{t,d} = q_{f,d}\, A_f \Big/ A_t \tag{2}$$

related to the value $q_{f,d}$ corresponding to the surface area of the floor

$$q_{f,d} = \frac{Q_{f,k}}{A_f} \cdot \delta_{q1} \cdot \delta_{q2} \cdot \delta_n \tag{3}$$

where: $Q_{f,k}$ is the characteristic fire load; δ_{q1} and δ_{q2} are dimensionless factors, taking into account the fire risk due to the size of the compartment and the type of occupancy, respectively; δ_n is a dimensionless factor taking into account the different fire fighting measures. With reference to 45 min (i.e. R45) and 60 min (i.e. R60) of exposure, the design parameters of the fire load reported in Table 3 are obtained, for the first and the upper levels of the test structure.

Fire compartment	Fire resistance [min]	$Q_{f,k}$ [MJ]	δ_{q1}	δ_{q2}	δ_n	$q_{f,d}$ [MJ/m^2]	$q_{t,d}$ [MJ/m^2]
First level	R45	102904	1	1	1	571.7	168.1
Upper levels		102904	1	1	1	571.7	185.1
First level	R60	114102	1	1	1	633.9	186.4
Upper levels		114102	1	1	1	633.9	205.2

Table 3: Design parameters of fire load.

Afterwards, the thermal absorptivity coefficient of the surrounding surfaces in the fire compartment can be calculated as

$$b = \sqrt{\rho c \lambda} \tag{4}$$

ρ being the density, c the specific heat and λ the thermal conductivity of enclosure boundary. More specifically, in the case the j-th enclosure surface is made with different layers of material, b_{1j} and b_{2j} thermal absorptivity coefficients should be adopted to define the design value b_j, where labels 1 and 2 refer to the layer directly exposed to the fire and the next one, respectively. Finally, to account for different thermal absorptivity coefficients in the walls (i.e. masonry infills), ceiling (i.e. top floor slab) and floor (i.e. bottom floor slab), the thermal absorptivity coefficient is modified thus:

$$b = \sum\nolimits_j \left(b_j \cdot A_j \right) \Big/ \left(A_t - A_v \right) \tag{5}$$

A_j being the area of the j-th enclosure surface, openings not included. In Table 4, the main parameters for defining the thermal absorptivity coefficient of the fire compartment are reported for the test structure, with reference to both R45 and R60 at the first and upper levels.

Fire compartment	Enclosure surface	b_{1j} [J/m^{2}s$^{1/2}$K]	b_{2j} [J/m^{2}s$^{1/2}$K]	b_j [J/m^{2}s$^{1/2}$K] R45	R60	A_j [m^2]	b [J/m^{2}s$^{1/2}$K] R45	R60
First level	Masonry infill	1131.37	963.00	1034.14	1030.56	228	1128.3	1125.8
	Top floor slab	1131.37	963.00	1034.14	1030.56	180		
	Bottom floor slab	1341.64	2300.00	1341.64	1341.64	180		
Upper levels	Masonry infill	1131.37	963.00	1034.14	1030.56	172	1138.2	1135.8
	Top floor slab	1131.37	963.00	1034.14	1030.56	180		
	Bottom floor slab	1341.64	2300.00	1341.64	1341.64	180		

Table 4: Thermal absorptivity coefficient of fire compartment.

Assuming closed openings once the fire scenarios have been hypothesized (Figure 1b), the temperature is considered uniform in the selected compartment (Figure 1a) in such a way to be the most severe condition for the fire before an earthquake. Several models can be used to simulate the time-temperature evolution during an actual fire, from the flashover to the full development: conventional fire curves (e.g. the standard ISO-834 curve [16]), in which the temperature monotonically increasing with time represents the heating phase only, when the fuel supply is assumed to be inexhaustible; natural fire curves (e.g. the EC1 curve [15]), in which temperature depends on the ventilation and fire load in the compartment and the cooling phase is represented, based on the assumption that at a certain point, either the air or the combustible material will diminuish.

The EC1 parametric fire curve is used in the present study, on the assumption that the fire load of the compartment is completely burnt out. In the heating phase, the gas temperature θ_g(°C)

$$\theta_g = 20 + 1325\left(1 - 0.324e^{-0.2t^*} - 0.204e^{-1.7t^*} - 0.472e^{-19t^*}\right) \tag{5}$$

is a function of a fictitious time t^* obtained by considering time t (in hours) multiplied by a dimensionless parameter equal to

$$\Gamma = \left(O/b\right)^2 \Big/ \left(0.04/1160\right)^2 \tag{6}$$

The gas temperature in the cooling phase is given by

$$\begin{aligned} &t^*_{\max} \le 0.5\ h \rightarrow \theta_g = \theta_{\max} - 625\left(t^* - t^*_{\max}\right) \\ &0.5\ h < t^*_{\max} < 2\ h \rightarrow \theta_g = \theta_{\max} - 250\left(3 - t^*_{\max}\right)\left(t^* - t^*_{\max}\right) \\ &t^*_{\max} \ge 2\ h \rightarrow \theta_g = \theta_{\max} - 250\left(t^* - t^*_{\max}\right) \end{aligned} \tag{7}$$

where the maximum temperature θ_{max} in the heating phase happens for

$$t^*_{\max} = \left(0.2 \cdot 10^{-3} q_{t,d} / O\right)\Gamma \tag{8}$$

Finally, the standard ISO-834 curve is defined as [16]

$$\theta_g = 20 + 345\log_{10}\left(8t + 1\right) \tag{9}$$

where t is expressed in hours.

With reference to the fire scenarios shown in Figure 1, the ISO and EC1 time-temperature curves are compared in Figure 2 in the case where a fire compartment is confined to the first level and the upper ones. The combination of fire parameters, for the open-plan office building, results in a temperature of 918°C (t^*_{max}=1.07h) and 942°C (t^*_{max}=1.27h) in 45 min (i.e.

fire resistance R45 in Figure 2a) and 816°C (t^*_{max}=1.19h) and 836 °C (t^*_{max}=1.41h) in 60 min (i.e. fire resistance R60 in Figure 2b), at the first and upper floors, respectively.

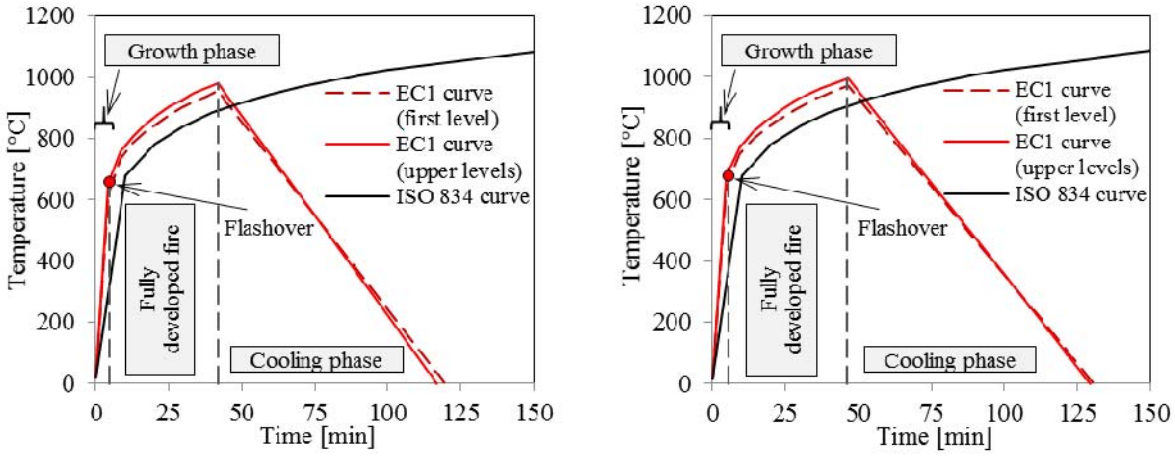

(a) R45. (b) R60.

Figure 2: Conventional (ISO 834) and natural (EC1) fire curves.

3 NUMERICAL RESULTS: FIRE LOADING BEFORE AN EARTHQUAKE

Once the time-temperature curve of the fire compartment is determined with the EC1 model, it is possible to evaluate the temperature distribution in the frame members of the test structure at R45 and R60. As an example, thermal mappings of interior and perimeter r.c. frame members in the first level of the test structure are plotted in Figure 3, considering a convection factor equal to 25 and an emissivity of the concrete surface equal to 0.56.

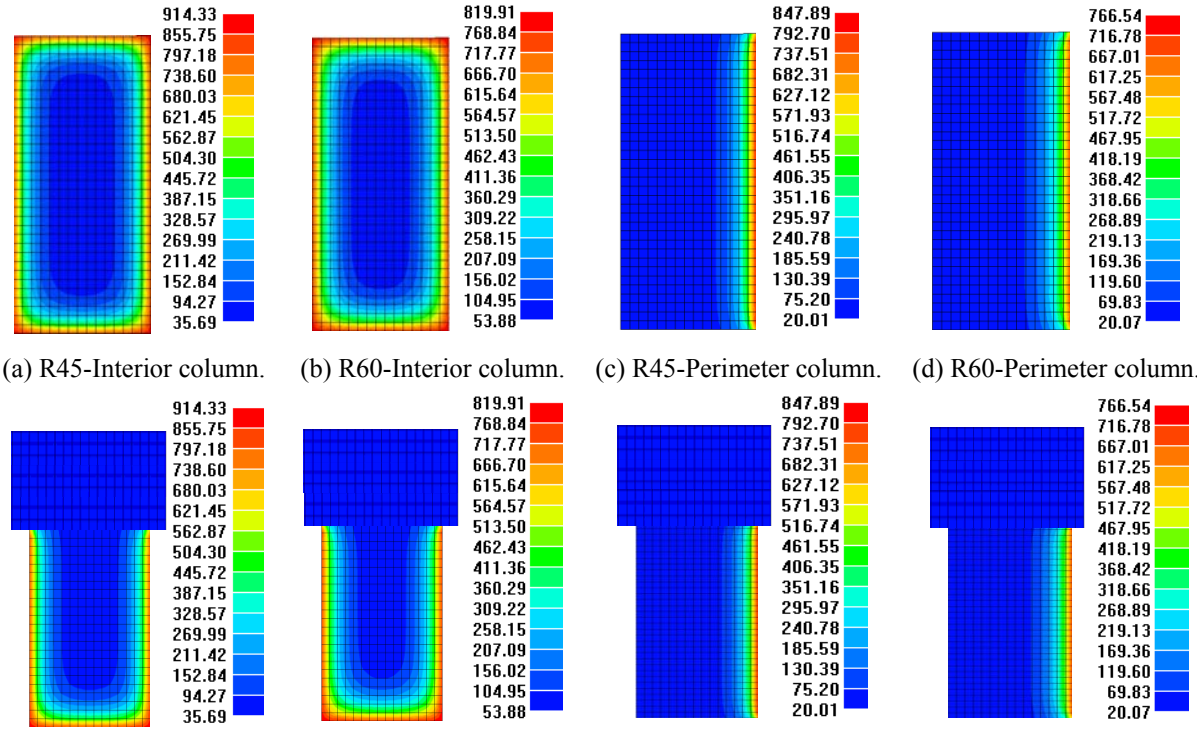

(a) R45-Interior column. (b) R60-Interior column. (c) R45-Perimeter column. (d) R60-Perimeter column.

(e) R45-Interior girder. (f) R60-Interior girder. (g) R45-Perimeter girder. (h) R60-Perimeter girder.

Figure 3: Thermal mappings at 1st level of test structure.

In detail, the finite thermal element cross-section model of columns, exposed to fire on four (Figures 3a and 3b) and one (Figures 3c and 3d) sides, and girders, exposed to fire on three (Figures 3e and 3f) and one (Figures 3g and 3h) sides, are considered assuming an ambient tempearture of 20°C for the unexposed cross-section sides. As expected, at the end of 45 and 60 minutes of exposure, the increase in temperature is greater in the case of cross-sections exposed on four or three sides compared to those exposed on one side only. Moreover, the temperature profiles highlight a decrease in the maximum value with the time increment from R45 to R60, in accordance with EC1 natural fire curves shown in Figure 2, but the concrete zone damaged by heat is more extended in the case of R60.

Subsequently, the residual seismic load capacity of the cross-sections after fire is evaluated in accordance with the 500°C isotherm method of Eurocode 2 [11], in terms of stiffness, strength and ductility reductions. The simplified calculation provides for a reduction of the cross-section size, with respect to a heat damaged zone defined by thermal mapping. Concrete with temperatures exceeding 500°C, corresponding roughly to the thickness of the unconfined zone, is not assumed to contribute, while the residual concrete cross-section retains its initial values of strength and modulus of elasticity. On the other hand, the reduced yield strength of each longitudinal reinforcement bar, in the tension and compression zones of the cross-section, is evaluated with respect to the steel temperature profile in the centre of the bar [17]. It is worth noting that some of the reinforcing bars may fall outside the reduced cross-section, but they are included in the calculation of the ultimate values of load bearing capacity and curvature ductility, which is evaluated in line with the provisions of Eurocode 8 for the assessment of existing buildings [18].

In Figure 4, flexural stiffness in the fire-exposed cross-section of r.c. frame members is reported along the building height, assuming a direct correspondence between the examined level and the fire compartment. In particular, interior columns (Figure 4a) and girders (Figure 4b) are examined at the end of 45 (i.e. F.R45 structure) and 60 (i.e. F.R60 structure) minutes of exposure to fire. As expected, a local decrease in stiffness from a minimum, of about 34% and 26% at the 1st level, and a maximum, of about 52% and 30% at the 5th level, is obtained for the interior columns and girders of the F.R45 structure, respectively, in comparison with the no-fire condition. A further minimum decrease in stiffness, of about 12% and 9% at the 1st level, and maximum, of about 13% and 10% at the 5th level, is obtained after an additional 15 minutes of fire (i.e. F.R60 structure). Further results, which are omitted for the sake of brevity, have confirmed limited fire effects in the perimeter frame members at all levels where the fire compartment is supposed.

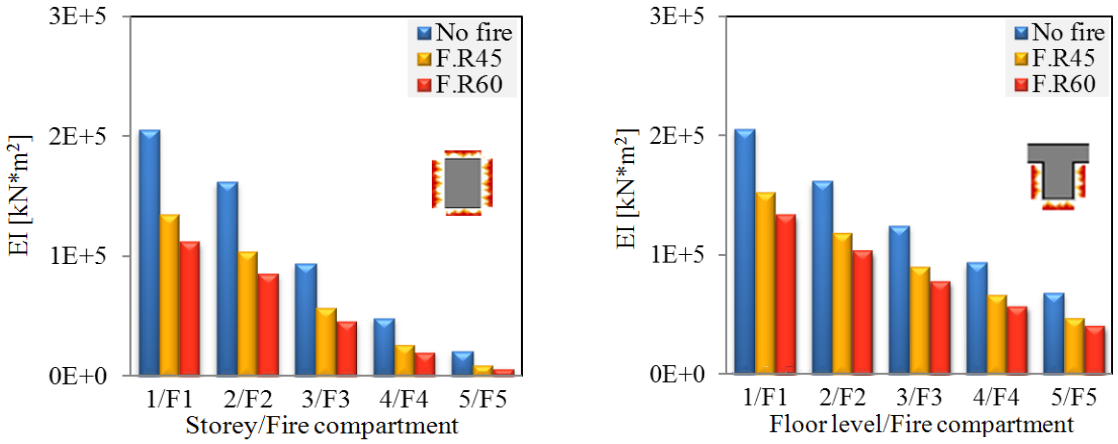

(a) Interior column n. 8. (b) Interior girder n. 3-8.

Figure 4: Flexural stiffness of r.c. frame members exposed to fire.

Thereafter, ultimate ductility of the columns, corresponding to the axial force due to the gravity loads, confirmed limited fire effects in the perimeter columns of all storeys where the fire compartment is supposed and a significant reduction only for the interior columns (Figure 5a), of about 22% and 33% for the F.R45 and F.R60 structures, respectively. Moreover, it is interesting to note that an increase of ductility is obtained on the bottom side of the interior girders (Figure 5b), of about 7% (i.e. F.R45) and 13% (i.e. F.R60), due to the fire-reduced yield strength of the longitudinal bars in tension. On the other hand, a decrease in the ultimate ductility at the top, of about 15% (i.e. F.R45) and 29% (i.e. F.R60), is observed because of heat damage to the compression zone of concrete and corresponding longitudinal reinforcement.

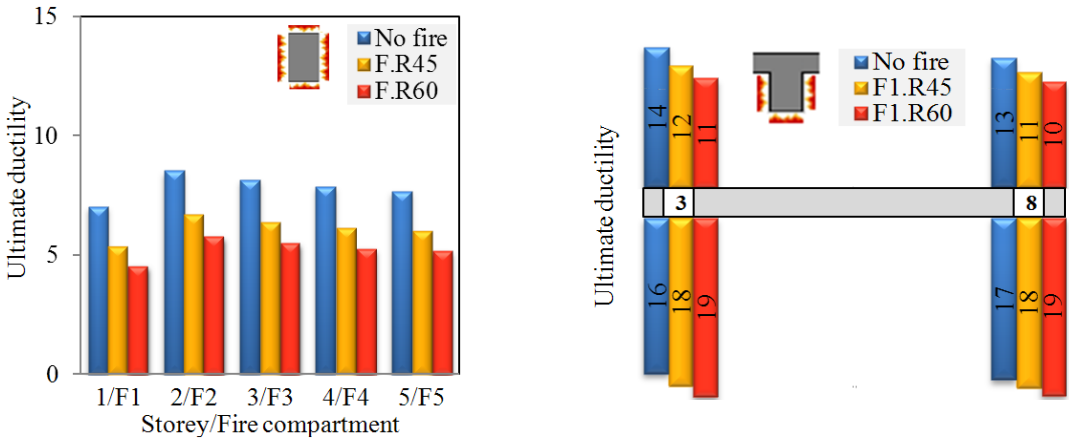

(a) Interior column n. 8. (b) Interior girder n. 3-8 (1st floor/F1).

Figure 5: Ultimate ductility of r.c. frame members exposed to fire.

Finally, analogous results are reported for the ultimate interaction domain between axial load (N_{Rd}) and bending moment (M_{Rd}) of columns (Figure 6) and the ultimate bending moment of girders (Figure 7). For clarity, only fire compartments at the first (i.e. F1 in Figures 6a and 7a) and fifth (i.e. F5 in Figures 6b and 7b) level are examined.

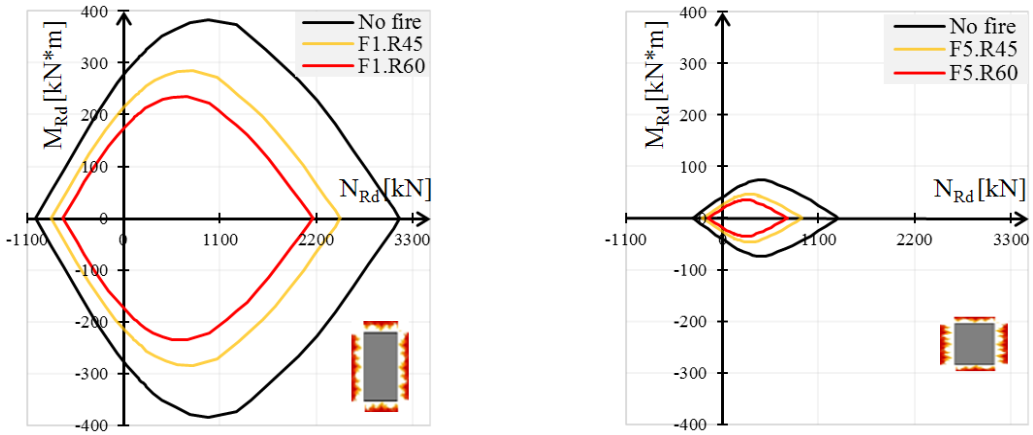

(a) Interior column n. 8 (1st storey/F1). (b) Interior column n. 8 (5th storey/F5).

Figure 6: Ultimate N_{Rd}-M_{Rd} domains of r.c. columns exposed to fire.

As can be observed, interior columns exhibit a marked narrowing of their N_{Rd}-M_{Rd} domains, especially for values of the compressive axial load greater than those corresponding to the balanced compressive load. For this axial load, a local reduction in flexural strength, in com-

parison with the no-fire condition, of about 26% and 39%, at the first storey, and 37% and 53%, at the fifth storey, is found in the F.R45 and F.R60 structures, respectively. On the other hand, a significant decrease in strength is observed on the bottom side of the interior girder 3-8 (see Figure 1a) with a maximum local reduction of about 35% and 55%, at the first floor, and 28% and 45%, at the fifth floor, considering the F.R45 and F.R60 structures, respectively.

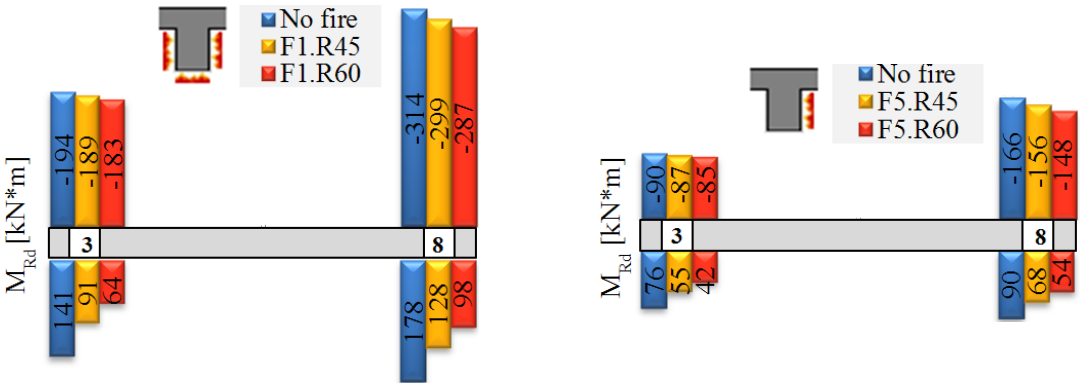

(a) Interior girder n. 3-8 (1st floor/F1). (b) Interior girder n. 3-8 (5th floor/F5).

Figure 7: Ultimate bending moments of r.c. girders exposed to fire.

4 NUMERICAL RESULTS: SEISMIC LOADING FOLLOWING FIRE

In order to study the seismic response of the r.c. framed building described in Section 2 and damaged according to the fire loading proposed in Section 3, nonlinear dynamic analyses are carried out. To this end, the r.c. frame members are idealized by means of a two-component model (TCM), constituted of an elastic-plastic component and an elastic component, assuming a bilinear moment-curvature law [19]. The effect of the axial load on the ultimate bending moment of the columns is also considered. At each step of the analysis, the elastic-plastic solution is evaluated in terms of the initial state and the incremental load on the basis of a holonomic law, as a solution of the Haar-Kàrmàn principle [20-22]. In the Rayleigh hypothesis, the damping matrix of the framed structure is assumed to be a linear combination of the mass and stiffness matrices, assuming a damping ratio of 5% with reference to the frequencies of the second and sixth vibration modes in the Y direction (see Table 1). In this way, a somewhat lower value of the damping ratio is achieved for the fourth mode in the same direction, while the higher frequency modes, which do not contribute significantly to the dynamic response, are practically eliminated due to their high damping ratio. The structural damage is evaluated in terms of ductility demand at the critical end sections (i.e. *i* and *j*) of girders and columns. The curvature ductility demand is calculated with reference to the two loading directions, assuming as yielding curvature for the columns that corresponding to the axial force due to the gravity loads.

Real ground motions corresponding to a high-risk seismic region provided by the current Italian seismic code (NTC08, [14]), and a design subsoil class *B* (i.e. subsoil stratigraphic parameter S_S=1.08) are considered. In detail, two sets of seven recorded accelerograms, selected by the computer code REXEL [23], are considered for the topographic classes *T1* and *T2* (i.e. topographic parameters S_{T1}=1.0 and S_{T2}=1.2). The corresponding elastic response spectra of normalized acceleration (S_a/g) are plotted in Figure 8, assuming an equivalent viscous damping ratio in the horizontal direction, ξ_H, equal to 5%, considering different scale factors (SFs). On average, these spectra match the corresponding target NTC08 response spectra for PGA_{T1}=0.34g (Figure 8a) and PGA_{T2}= 0.41g (Figure 8b), in the range of vibration periods 0.05s–4s, which also contains the lower and upper limits of the vibration period (i.e. T_{min}=0.2T_1 and T_{max}=2T_1, where T_1 is the fundamental vibration period of the structure). Thus,

the selected accelerograms can be used for the nonlinear dynamic analysis of structures with $T_1 \leq 1$s. All the following results are obtained as an average of those separately obtained for the sets *T1* and *T2* of real motions.

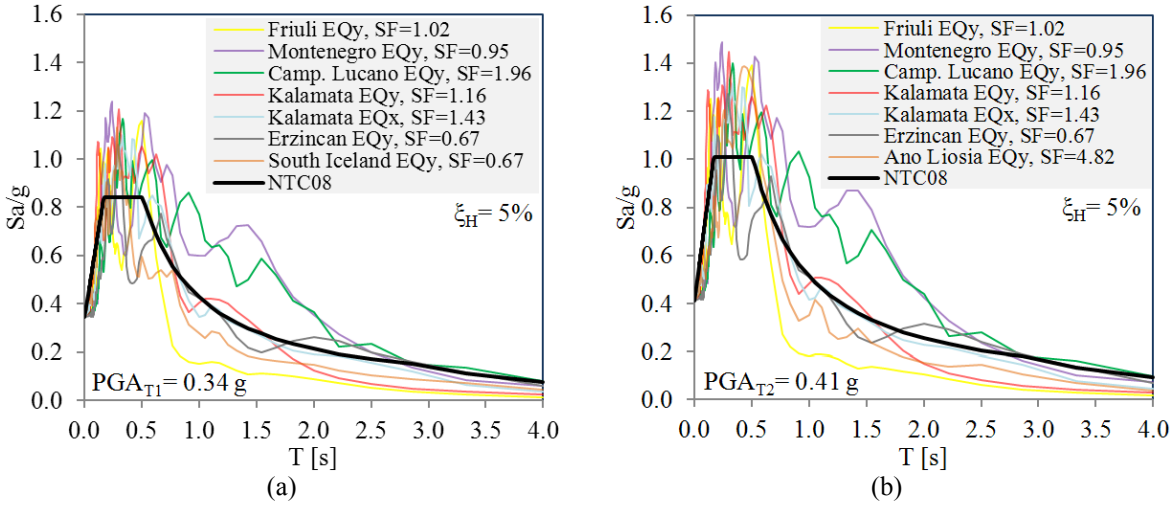

Figure 8: Acceleration (elastic) response spectra for the topographic classes *T1* (a) and *T2* (b).

Firstly, maximum ductility demand of columns and girders along the building height is plotted in Figure 9, for the topographic class *T1* (i.e. PGA_{T1}=0.34g), comparing framed structures both in the no-fire condition and at the end of 45 (i.e. R45) and 60 (i.e. R60) minutes of fire exposure. More specifically, interior columns (Figures 9a and 9c) and girders (Figures 9b and 9d) are examined, on the assumption that the fire compartment is confined to the area of the first (i.e. F1, Figures 9a and 9b) and the fourth (i.e. F4, Figures 9c and 9d) levels.

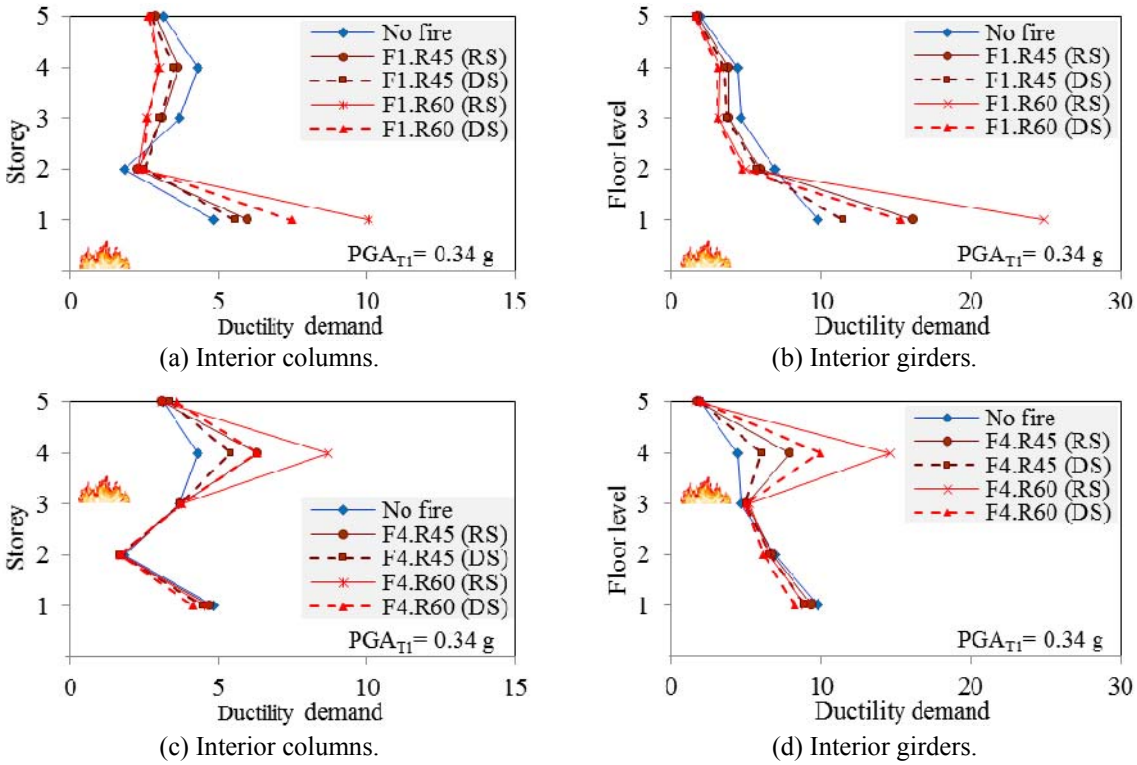

Figure 9: Global ductility demand for the topographic class *T1*:
(a) and (b), fire at the 1st level (fire scenario F1); (c) and (d), fire at the 4th level (fire scenario F4).

Moreover, r.c. frame members are assumed to have been previously damaged by fire, with a reduced cross-section (i.e. in the Damaged Stiffness condition, DS), and later repaired, e.g. using jacketing with thin layers of concrete (i.e. in the Repaired Stiffness condition, RS). As can be observed, an amplification in the structural response of fire-exposed structures is localized to the level of the fire compartment involved. As expected, this result is more marked in the F1.R60 and F4.R60 structures than in the F1.R45 and F4.R45 ones, because the first are characterized by lower strength and ductility. The results also show that the seismic response of the test structures differs in the DS and RS conditions, with higher ductility demand when the initial stiffness is restored (i.e. RS condition).

To better clarify the local damage distribution, top (i.e. μ_{Ti} and μ_{Tj}) and bottom (i.e. μ_{Bi} and μ_{Bj}) maximum ductility demand in the frame members and corresponding ultimate values are reported in Figure 10 for the fire scenarios F1 (Figures 10a and 10b) and F4 (Figures 10c and 10d). In particular, girders and columns exposed to fire on three (e.g. the interior girder 3-8) and four (e.g. the interior column 8) sides are examined. Note that the maximum ductility demand and the number of sections in which the corresponding ultimate value is exceeded increase especially at the first level, with an amplification when the initial stiffness is restored (i.e. RS condition) and R60 is assumed (Figures 10a and 10b). In this case, three interior columns and all interior girders exceed the corresponding ultimate ductility demand at the first level. Moreover, a significant increase of ductility demand on the fourth level is observed only in the interior columns of the F4.R60 structure (Figure 10c), producing a "strong beam-weak column mechanism" at this level. Further results, omitted for the sake of brevity, have confirmed this behaviour also in the case of the F3 and F5 fire scenarios.

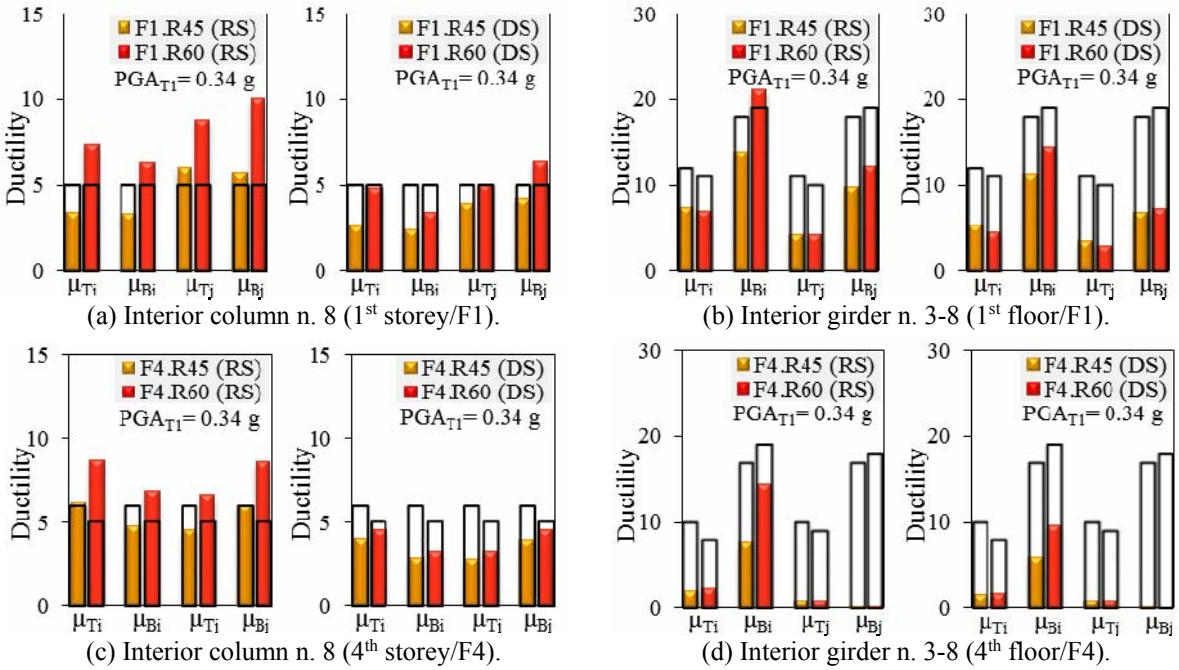

(a) Interior column n. 8 (1st storey/F1). (b) Interior girder n. 3-8 (1st floor/F1).

(c) Interior column n. 8 (4th storey/F4). (d) Interior girder n. 3-8 (4th floor/F4).

Figure 10: Local ductility for the topographic class T1:
(a) and (b), fire at the 1st level (fire scenario F1); (c) and (d), fire at the 4th level (fire scenario F4).

Afterwards, taking into account the symmetric plan shown in Figure 1a, the distribution of maximum ductility demand in the perimeter and interior frame members is investigated in Figure 11. Local maximum ductility demand in the perimeter and interior columns (Figures 11a and 11c) and girders (Figures 11b and 11d) for the DS (Figures 11a and 11b) and RS (Figures 11c and 11d) conditions are plotted at the first level where the fire compartment is

hypothesized. Note that the ductility demand increases especially in the frame members exposed on three (i.e. the interior girders 2-7, 7-12, 3-8 and 8-13) and four (i.e. the interior columns 7 and 8) sides in the RS condition. Moreover, among the columns exposed on one side greater ductility demand is obtained in the perimeter ones of the exterior frames (i.e. the perimeter columns 1, 6 and 11). Further results, omitted for the sake of brevity, confirm an increase of maximum ductility demand and number of frame members in which the corresponding ultimate value is exceeded, especially at the lower storeys.

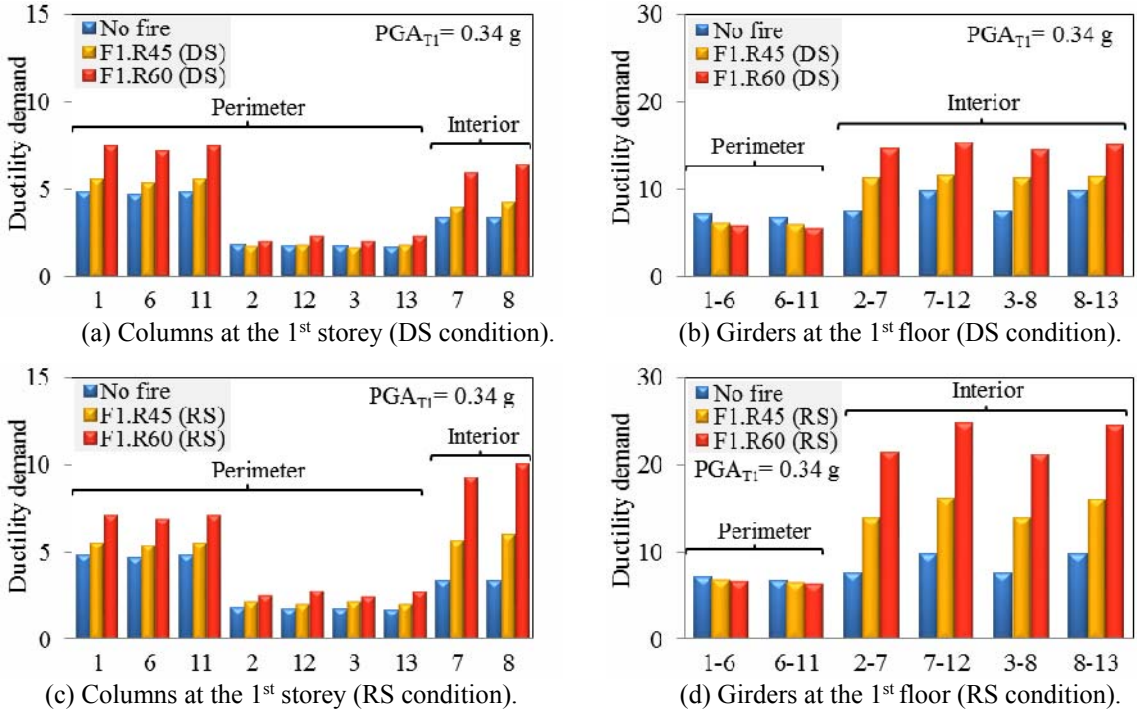

(a) Columns at the 1st storey (DS condition).

(b) Girders at the 1st floor (DS condition).

(c) Columns at the 1st storey (RS condition).

(d) Girders at the 1st floor (RS condition).

Figure 11: Local ductility demand for the topographic class *T1*: fire at the 1st level (fire scenario F1).

Finally, curves analogous to those above reported are shown in Figure 12 where fire compartment is confined to the area of the first two levels (i.e. F1/2 scenario) and R60 is assumed, with reference to the topographic classes *T1* (i.e. PGA_{T1}=0.34g) and *T2* (i.e. PGA_{T2}=0.41g). As can be observed, a significant increase in ductility is obtained in the frame members of the fire compartment moving from *T1* to *T2* topographic class.

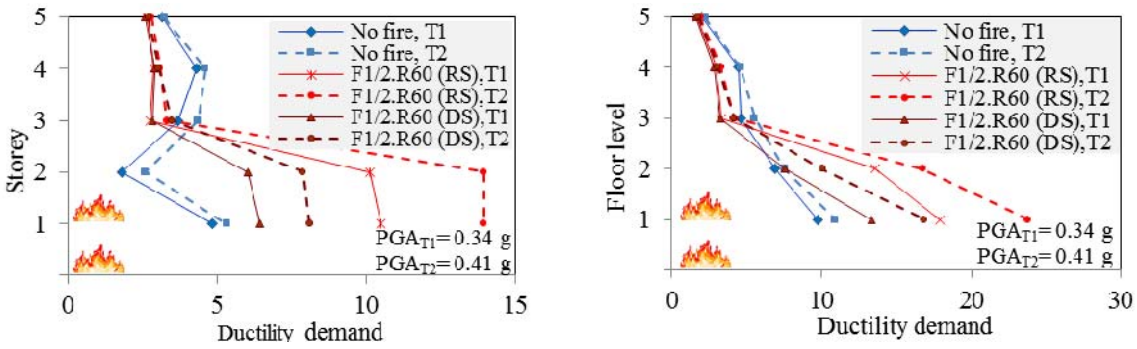

(a) Interior columns.

(b) Interior girders.

Figure 12: Global ductility demand for the topographic classes *T1* and *T2*: fire at the 1st and 2nd levels (fire scenario F1/2).

Moreover, the maximum ductility demand of the interior columns (Figure 12a) and girders (Figure 12b) increases at the levels where the event of fire is hypothesized while it is reduced, in comparison with the no fire conditions, on the other levels. This behaviour is amplified when the RS condition and topographic class *T2* are considered. In this case, the ultimate ductility demand is reached in all the interior columns of the first two levels and all the interior girders of the first one.

5 CONCLUSIONS

The nonlinear seismic response of five-storey r.c. framed buildings, primarily designed in line with the previous Italian seismic code for a medium risk zone, is studied under two sets of seven real motions whose response spectra match, on average, NTC08 spectra with regard to a high-risk seismic zone and two topographic classes. More specifically, the nonlinear dynamic analysis of framed structures in a no fire situation is compared with that in the event of fire, at 45 (i.e. R45) and 60 (i.e. R60) minutes of exposure to fire, assuming both damaged (i.e. DS) and repaired (i.e. RS) stiffness conditions.

The numerical results show that fire safety should also be taken into account when evaluating the seismic vulnerability of existing r.c. framed buildings. Fire results show a significant decrease in stiffness and ultimate values of strength and ductility in the interior columns and girders and negligible effects in the perimeter ones. Seismic results highlight an amplification in the structural response localized to the level where the fire compartment is hypothesized, with a slight reduction on the other levels in comparison with the no fire condition. Moreover, fire scenarios at the upper levels produce "strong beam-weak column" local mechanism at these levels. Finally, the results show that the seismic vulnerability of the test structure differs in the DS and RS conditions, with higher ductility demand in the case where the initial stiffness has been restored.

ACKNOWLEDGEMENTS

The present work was also financed by Re.L.U.I.S. (Italian network of university laboratories of earthquake engineering), according to "Convenzione D.P.C.–Re.L.U.I.S. 2014–2016, WPI, Isolation and Dissipation".

REFERENCES

[1] C. Scawthorn, J.M. Eidinger, A. Schiff, Fire following earthquake. New York, NY *American Society of Civil Engineers*, 2005.

[2] V.K.R. Kodur, M. Garlock, N. Iwankiw, Structures in fire: state-of-the-art, research and training needs, *Fire Technology*, **48**, 825-839, 2012.

[3] H. Mostafaei, T. Kabeyasawa, Performance of a six-story reinforced concrete structure in post-earthquake fire. Institute for Research in Construction, *10th Canadian Conference on Earthquake Engineering*, Toronto, Canada, July 25-29, **1**, 481-490, 2010.

[4] B. Behnam, H. Ronagh, Performance of reinforced concrete structures subjected to fire following earthquake. *European Journal of Environmental and Civil Engineering,* **17**(4), 270-292, 2013.

[5] V.K.R. Kodur, N.K. Raut, X.Y. Mao, W. Khaliq, Simplified approach for evaluating residual strength of fire-exposed reinforced concrete columns. *Materials and Structures*, **46**, 2059-2075, 2013.

[6] H. Mostafaei, F. Vecchio, N. Bénichou, Seismic Resistance of Fire-Damaged Rein-

forced Concrete Columns. *ATC and SEI Conference on Improving the Seismic Performance of Existing Buildings and Other Structures,* San Francisco, California, United States, December 9-11, **1**, 1396-1407, 2009.

[7] F. Mazza, F. Alesina, Incremental dynamic analysis of fire-exposed base-isolated r.c. framed buildings subjected to near-fault ground motions. *COMPDYN 2015, 5th ECCOMAS Thematic Conference on Computational Methods in Structural Dynamics and Earthquake Engineering*, Crete Island, Greece, May 25–27, paper n. 492, 2015.

[8] H. Mostafaei, Hybrid fire testing for assessing performance of structures in fire - Methodology. Fire Safety Journal, **58**, 170-179, 2013.

[9] H. Mostafaei, Hybrid fire testing for assessing performance of structures in fire - Application. Fire Safety Journal, **56**, 30-38, 2013.

[10] Italian Ministry of Public Works (DM96). Norme tecniche per le costruzioni in zone sismiche e relative istruzioni, D.M. 16-01-1996 and C.M. 10-04-1997, n. 65/AA.GG..

[11] Eurocode 2. Design of concrete structures – Part 1-2: General rules, structural fire design. *C.E.N., European Committee for Standardization*, December 2004.

[12] F. Mazza, A. Vulcano, Nonlinear dynamic response of r.c. framed structures subjected to near-fault ground motions. *Bulletin of Earthquake Engineering*, **8**, 1331-1350, 2010.

[13] F. Mazza, M. Mazza, Nonlinear modeling and analysis of R.C. framed buildings located in a near-fault area. *The Open Construction & Building Technology Journal,* **6**, 346-354, 2012.

[14] Italian Ministry of Infrastructures (NTC08). Nuove norme tecniche per le costruzioni e relative istruzioni, D.M.14-01-2008 e Circolare 02-02-2009, n. 617/C.S.LL.PP..

[15] Eurocode 1. Actions on structures – Part 1-2: General actions, actions on structures exposed to fire. *C.E.N., European Committee for Standardization*, October 2004.

[16] ISO 834 International Standard, Fire resistance tests, ISO 834-1 Test conditions. *Provided by IHS under license with ISO: 31*, Genève, Switzerland, 1999.

[17] F. Mazza, M. Fiore, Comparative study of the wind and earthquake dynamic responses of fire exposed steel framed buildings. *COMPDYN 2015, 5th ECCOMAS Thematic Conference on Computational Methods in Structural Dynamics and Earthquake Engineering*, Crete Island, Greece, May 25–27, paper n. 490, 2015.

[18] Eurocode 8. Design of structures for earthquake resistance – Part 3: Assessment and retrofitting of buildings. *C.E.N, European Committee for Standardization*, June 2004.

[19] F. Mazza, Modelling and nonlinear static analysis of reinforced concrete framed buildings irregular in plan. *Engineering Structures*, **80**, 98-108, 2014.

[20] F. Mazza, M. Mazza, Nonlinear analysis of spatial framed structures by a lumped plasticity model based on the Haar-Kàrmàn principle. *Computational Mechanics*, **45**, 647-664, 2010.

[21] F. Mazza, A distributed plasticity model to simulate the biaxial behaviour in the nonlinear analysis of spatial framed. *Computers and Structures*, **135**, 141-154, 2014.

[22] F. Mazza, M. Mazza, Nonlinear modeling and analysis of r.c. spatial frames to study the effects of the vertical component of near-fault ground motions. *COMPDYN 2015, 3rd ECCOMAS Thematic Conference on Computational Methods in Structural Dynamics and Earthquake Engineering*, Corfù, Greece, May 25–28, paper n. 322, 2013.

[23] I. Iervolino, G. Maddaloni, E. Cosenza, Eurocode 8 compliant record sets for seismic analysis of structures. *Journal of Earthquake Engineering*, **12**, 54–90, 2008.